Continuous supercritical synthesis of high quality UV-emitting ZnO nanocrystals for optochemical applications

Evgeniy S. Ilin, Samuel Marre, Veronique Jubera, Cyril Aymonier

PAPER

Continuous supercritical synthesis of high quality UV-emitting ZnO nanocrystals for optochemical applications

Evgeniy S. Ilin,[ab] Samuel Marre,[ab] Véronique Jubera[ab] and Cyril Aymonier*[ab]

ZnO nanocrystals (NCs) are of increasing interest in many industrial applications especially in the field of optochemical sensors. We recently demonstrated the synthesis of excitonic luminescent ZnO NCs using the perfectly controlled environment offered by supercritical microfluidics. However, the limited production rates of such a microscale synthesis approach make it essential to develop scaled-up continuous supercritical synthesis processes. Here, we investigate the influence of the scale-up effect from continuous microfluidic up to millifluidic systems over the synthesized ZnO NCs' optical properties. We also propose to discuss the influence of reactor's dimensions, as a consequence of different hydrodynamics regimes, on the characteristics of ZnO NCs. The obtained ZnO NCs have various shapes depending on the considered set-up. A strong excitonic-only emission in the UV region in room temperature photoluminescence (PL) spectra is obtained from all types of reactors, demonstrating the success of the scale-up process for higher production rates (up to 100 mg per hour).

DOI:10.1039/XXXXXXXXX

Introduction

Zinc oxide (ZnO) is a well-known and deeply investigated material with many applications in different fields such as piezoelectric transducers, optical waveguides, surface acoustic wave devices, transparent conductive oxides, and photocatalysis.[1–4] In recent years, high-efficiency UV photoluminescence (PL) of ZnO nanostructures has been intensively investigated for the development of new devices such as gas sensors,[5] light-emitting diodes,[6] lasers,[7] and DNA sensors, which are usable in the biomedical field.[8] Numerous methods have been studied for the synthesis of ZnO nanostructures such as chemical vapor deposition,[9] precipitation,[10] sol–gel,[11] inverse microemulsion,[12] organometallic route,[13] solvothermal[14] or still supercritical fluid approaches.[15]

The ZnO nanostructures liquid phase synthesis methods at low operating temperatures allow obtaining ZnO nanostructures with controlled size, size distribution and morphology. However, such ZnO nanostructures usually exhibit a broad emission band in the PL spectra visible domain centered at $\lambda = 500$–600 nm (2.07–2.48 eV).[16] The origin of this emission is attributed to the surface and bulk defects, resulting from low synthesis temperatures. Such PL properties make these ZnO nanostructures unusable for most applications such as light-emitting diodes. Conversely, high-temperature gas-phase synthesis methods allow the creation of ZnO materials with intense emission in the PL spectra UV domain.[17] This emission is typically located at $\lambda = 370$–380 nm (3.35–3.43 eV) and is due to radiative excitonic recombination.[18] However, these methods make size control of ZnO nanostructures very difficult.[19] Recently, supercritical fluids processing within hydrodynamically controlled environments offered by high pressure/high temperature microreactors (namely supercritical microfluidics – SCμF[20–22]) has given the opportunity to design excitonic luminescent ZnO NCs. These ZnO NCs were obtained through the transformation of zinc acetylacetonate in the presence of hydrogen peroxide in supercritical ethanol using an original co-flowing microfluidic process.[23] Although supercritical microfluidics allows the development of new processes for high quality NCs, production rates remain very low (few mg per hour). The synthesized excitonic-only ZnO NCs could be the active elements of future optochemical sensors. Therefore, in order to realize the promising applications of these devices, it will be critical to have a larger production scale.

We report here the development of supercritical fluid based millifluidic continuous synthesis of high quality ZnO NCs. We are mainly investigating the influence of reactor dimensions associated with hydrodynamics on the characteristics of ZnO NCs and their photoluminescence properties.

Experimental

Materials

All chemicals, including zinc acetylacetonate monohydrate ($Zn(acac)_2 \cdot H_2O$), hydrogen peroxide (H_2O_2 – 35 wt% in water),

[a]CNRS, ICMCB, UPR 9048, F-33600 Pessac, France. E-mail: aymonier@icmcb-bordeaux.cnrs.fr; Fax: +33 540002761; Tel: +33 540002672

[b]Univ. Bordeaux, ICMCB, UPR 9048, F-33600, Pessac, France. Fax: +33 540002761; Tel: +33 540002672

trioctylphosphine (TOP, purity of 90%) and absolute ethanol, were purchased from Sigma-Aldrich and used as received.

Synthesis of ZnO nanocrystals

Details of the supercritical microfluidics based experimental set-up and the operating procedures are described elsewhere.[23] In this paper, modifications are introduced concerning the size of each tubing forming the co-flowing micro- and millireactors (Fig. 1).

We have developed four different co-flowing systems (C_1 to C_4) allowing switching from micro- up to a millifluidics to reach a gram scale production range per day. Reactors are heated using an oil bath ($T = 250$ °C) and pressure is controlled with a back-pressure regulator downstream ($p = 25$ MPa). The first solution S_1 (Fig. 1) which contains $Zn(acac)_2 \cdot H_2O$ precursor (10^{-2} M) and H_2O_2 (2×10^{-2} M) in absolute ethanol is injected into the internal capillary (corresponding to a ratio $H_2O_2/Zn = 2/1$). The second solution S_2, consisting of trioctylphosphine (TOP) in absolute ethanol (6×10^{-2} M), is injected through the external capillary (molar ratio Zn/TOP = 1/6). The residence time was fixed at 10 s for C_1, C_2 and C_3 co-flow microreactors based on our previous studies.[23] In the case of the C_4 co-flow millireactor, the residence time was increased up to 40 s to obtain the right temperature profile in the reactor.[24] The ZnO NCs in ethanol are recovered downstream the back-pressure regulator. The ZnO NCs produced with C_1–C_3 microreactors were recovered by centrifugation at 9000 rpm and dried under air for 5 h. In the case of the C_4 millireactor, the ZnO NCs were recovered by simple Büchner filtration.

The increasing quantity of produced ZnO NCs allows access to new characterization techniques (Table 1). In the case of the C_1 and C_2 microreactors synthesis, only Raman spectroscopy and electronic diffraction could be used for the structural characterization of ZnO NCs. However, with a larger amount of ZnO powder, the structural, thermal and the other properties of ZnO NCs could be deeply investigated.

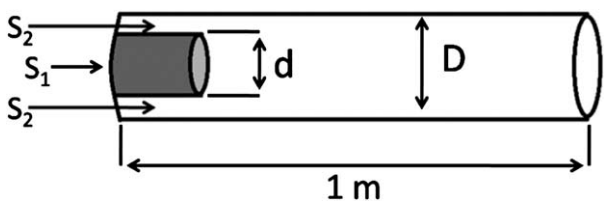

Fig. 1 Scheme of co-flow reactors developed for this study.

Characterization of ZnO NCs

Raman spectra were obtained using a Thermo scientific DXR micro-Raman spectrometer with a 532 nm excitation wavelength and a laser power of 10 mW. Raman spectroscopy was used to determine the structure of ZnO nanopowders, especially when using C_1 and C_2 configurations, for which the powder quantities were too small to perform XRD characterization. The routine X-ray diffraction measurements (XRD) were recorded with a PANalytical X'Pert Pro powder diffractometer in the Bragg–Brentano geometry using a monochromator with $K\alpha_1$ line ($\lambda = 1.54056$ Å) for C_3 and C_4 configuration samples at room temperature over the angular 2θ range 8–80 degrees with a step of 0.02 degree. The samples were prepared by depositing ZnO powder on a silicon substrate. High-resolution X-ray diffraction measurements were collected at room temperature over the angular 2θ range 20–120 degrees with a step of 0.02 degree. Rietveld refinement was carried out using the FullProf program for pure ZnO NCs and also for the ZnO–α-Al_2O_3 mixture to evaluate the crystallinity of the samples.[25] Single crystal data from ICSD database for ZnO and α-Al_2O_3 were used as the initial model.[26] The size, shape and polydispersity of ZnO NCs were observed by High-Resolution Transmission Electron Microscopy (HRTEM). Samples for HRTEM were prepared by dropping the ZnO powder suspension in ethanol on a copper carbon grid. HRTEM observations were performed using a JEOL 2200 FS equipped with a field emission gun, operating at 200 kV and with a point resolution of 0.23 nm. FTIR spectra for all samples were recorded using a Bruker FTIR Infrared spectrometer for achieving absorption and reflection from 7500 to 400 cm^{-1}. The ZnO powders were mixed with KBr and deposited on the steel support. The weight percentage of organics covering the ZnO NCs surface was determined by Thermogravimetric Analysis (TGA). Solid samples of approximately 5 mg were characterized using a Pyris™ 1 TGA analyzer (PerkinElmer) at a heating rate of 6 °C min^{-1} in the temperature range of 20–600 °C under a N_2 atmosphere. X-ray Photoelectron Spectroscopy (XPS) spectra were measured with an ESCALAB 220iXL from VG, a RX source TWIN Mg (1253.6 eV) and a scanning power of 150 eV. The analyzed area is a circle with a diameter of 150 μm. High resolution spectra were obtained with an energy E_p of 40 eV. The samples were prepared by pressing a small amount of powder on indium foils. Spectra were exploited with the AVANTAGE software from Thermo Fisher Scientific. The photoluminescence measurements at room temperature have been carried out with a Jobin Yvon SPEX spectrofluorometer (Fluorolog 212) and a SPEX 1680 0.22m Double Spectrometer

Table 1 Dimension and hydrodynamic parameters of the reactors (*average velocity ratio of external to internal flow)

Scale	Reactor	d (μm)	D (μm)	Flow rate ratio	R_H*	Reynolds number (after the contacting point)	Average production rate (mg h^{-1})	Available characterization techniques
Micro	C_1	100	250	2.75	1.22	45	3	Raman, PL, TEM
	C_2	100	320	2.74	0.44	57	5	Raman, PL, TEM
	C_3	250	750	2.78	0.40	132	30	Raman, PL, TEM, XRD
Milli	C_4	750	2100	2.78	0.85	32	100	Raman, PL, TEM, XRD, IR, TGA

equipped with a double monochromator and a xenon lamp. Emission spectra were corrected from the sensibility of the detector, the lamp flux and the collection geometry. The ZnO NC samples for PL measurements were prepared by depositing ZnO powder on a quartz plate or by dropping an ethanol suspension of ZnO NCs.

Results and discussions

ZnO NCs are formed by decomposing $Zn(acac)_2 \cdot H_2O$ in the presence of H_2O_2 in supercritical alcohol at 250 °C and 25 MPa.[23]

The crystal structure of ZnO NCs synthesized with the four co-flow reactor configurations (Fig. 2a) was investigated by Raman spectroscopy (Fig. 2b). The nonpolar optical phonon mode E_2, which is active in the case of all samples, has the most intensive and narrow peak around 436 cm^{-1}, corresponding to the würtzite type structure of ZnO.[27] The polar $A_1(TO)$ located at 326–335 cm^{-1} and E_1 at 411–417 cm^{-1} modes of the hexagonal, würtzite structure of ZnO are also visible in all cases instead of $A_1(LO)$ at 576 cm^{-1} mode, which is observed only in the case of samples produced with C_3 and C_4 type reactors. Raman spectroscopy performed on samples obtained with all types of reactors confirms that ZnO NCs exhibit the würtzite-type structure.

Fig. 2c shows PL spectra of ZnO NCs obtained from all types of reactor configurations. Only one narrow line at 377 nm is observed. This UV-emission is attributed to the excitonic recombination. In the meantime, there is no emission in the visible domain of the spectra, which reveals that there is no evident bulk and surface defect emission. This process makes it possible to produce nanoscale size particles with luminescent properties similar to those observed for high temperature gas phase synthesis processes. The structural properties of ZnO NCs obtained from C_3 and C_4 type reactors were characterized by XRD thanks to higher amounts of produced ZnO NCs powder available from these larger scale experimental configurations (Fig. 3). All diffraction peaks can be attributed to the ZnO würtzite hexagonal structure.[28] Furthermore, satisfying values of Rietveld refinement (Fig. 3b) indexes in agreement with the würtzite-type structure of ZnO are reached (Bragg *R*-factor – 5.3,

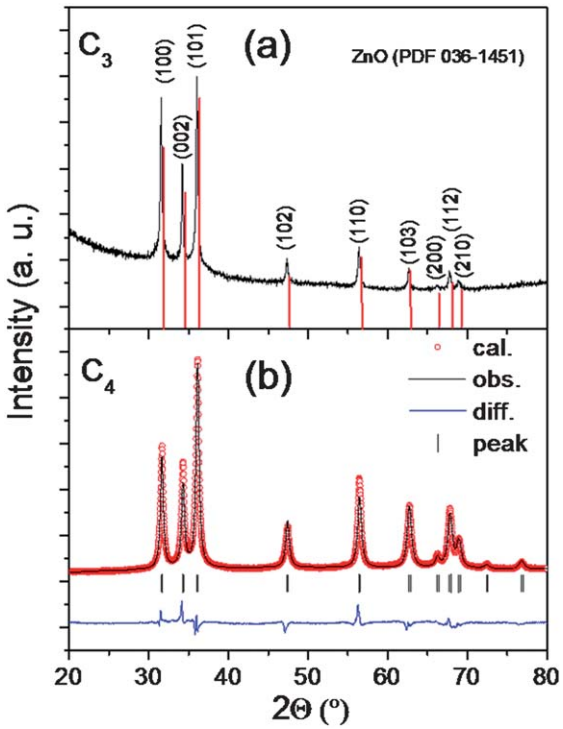

Fig. 3 XRD patterns of ZnO NCs obtained with a C_3 microreactor (a) and Rietveld refinement of the XRD patterns obtained with a C_4 millireactor (b).

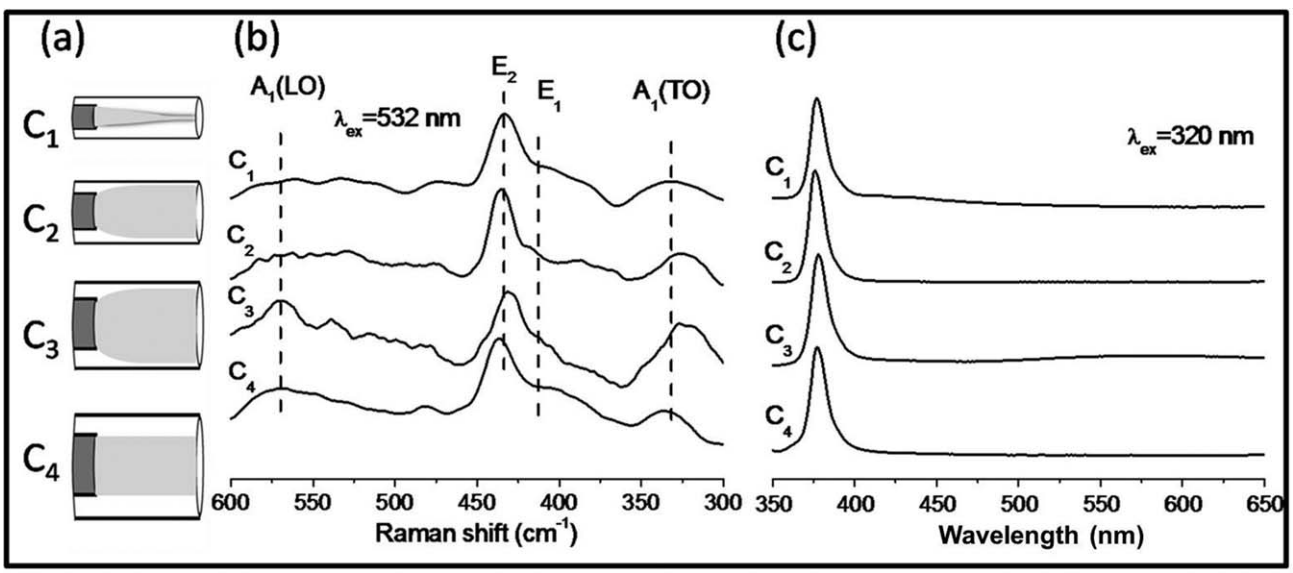

Fig. 2 Scheme of the internal flow regimes depending on reactors' configuration (a) Raman (b) and photoluminescence spectra (c) of ZnO NCs obtained from all types of reactors.

RF-factor – 3.2). The values of the refined lattice parameters are $a = b = 3.2512(1)$ Å, $c = 5.2090(2)$ Å and cell volume (V) = 47.687(3) Å^3. Rietveld refinement of a mixture of 50 wt% α-Al_2O_3 with 50 wt% ZnO obtained from the C_4 type reactor shows that ZnO NCs are highly crystalline (only 0.5% of amorphous ZnO). The high resolution TEM micrograph (Fig. 4) shows a spherical ZnO NC with size around 9 nm (C_4 millireactor). The lattice spacing was measured to be 1.9 Å from the zoomed inset image, which corresponds to the distance between two (102) planes of the ZnO structure. However, ZnO NCs with different crystallographic planes such as (110), (103) or (100) were also observed (data not shown here).

Furthermore, ZnO NCs obtained with all types of reactors have the same excellent optical properties – emission only in the PL spectra UV domain without any visible emission, confirming their high crystallinity. Thereby, the resulting Raman and PL spectra of all samples make it possible to confirm that ZnO NCs obtained with milliscale reactors have the same structural and optical properties as ZnO NCs obtained with microscale reactors. This methodology is presented for the first time: a supercritical microfluidics approach for developing a new process for synthesizing high quality excitonic luminescent ZnO NCs, then the development of a continuous supercritical synthesis at a larger scale providing the same material quality.

The size, size distribution and shape of ZnO NCs were further investigated by HRTEM. Fig. 5 shows the micrographs of ZnO NCs obtained from all types of co-flow reactor configurations. ZnO NCs obtained from the C_1 type microreactor exhibit two ZnO NCs morphologies – spherical NCs with a main size of 3.8 nm and also triangular nanoparticles. Two different ZnO NCs shapes are equally obtained with C_3. In this case, spherical ZnO NCs with an average size of 4.7 nm and ZnO nanorods are observed. With C_2 and C_4 co-flow reactors, only spherical ZnO NCs are observed with sizes of 6.1 and 9.4 nm, respectively.

These dependencies in size and shape of ZnO NCs could be discussed from the difference in hydrodynamic regimes occurring in the different co-flow reactors. Table 1 shows several hydrodynamic parameters such as capillary size, flow rate ratio, Reynolds number and also the calculated average velocity ratios of external to internal flow (R_H). The R_H value for all types of co-flow reactors was calculated with the following equation:

$$R_H = \frac{Q_{ext}}{Q_{int}} \frac{S_{int}}{S_{int} - S_{ext}}$$

where Q_{ext} and Q_{int} are the external and internal flow rates, and S_{ext} and S_{int} are the external and internal cross-sectional area of reactors, respectively. One can notice that in all configurations, the flow is laminar. The shape of the internal flow depends on the R_H parameter value. Two main regimes could appear depending on the R_H value – the flow focusing regime ($R_H > 1$) and the flow spreading regime ($R_H < 1$).[23] Fig. 2a shows the typical shapes of the internal precursor solution flow for the different reactor configurations. The flow focusing regime ($R_H > 1$) is observed in the case of the C_1 reactor. On the other side, C_2 and C_3 reactors are in the flow spreading regime ($R_H < 1$) and C_4 is intermediate between these two hydrodynamic regimes. Regarding these, it makes it possible to have ZnO NCs with different sizes and shapes keeping all other operating parameters constant (oxidant to zinc ratio $R_{Ox} = 2/1$, zinc to TOP ratio $R_L = 1/6$, temperature, pressure and residence time) just by changing the reactors' geometry through the capillaries dimensions. So, we assume that the hydrodynamic regime could have an influence on the nucleation and growth of ZnO NCs mainly through the interaction between TOP (external flow) and NCs in growth (internal flow). Studies are in progress to better understand the correlation between reactors' hydrodynamic regime and ZnO NCs size and morphology. Besides the continuous synthesis of excitonic luminescent ZnO NCs, our approach also allows the production of ZnO NCs with different sizes and morphologies.

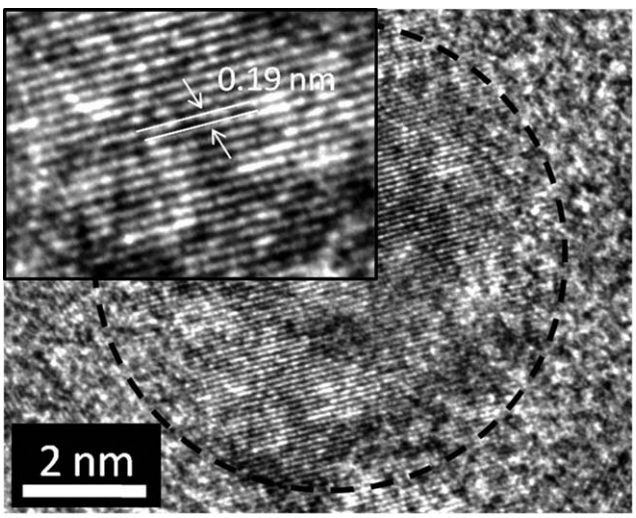

Fig. 4 High-magnification HR TEM micrograph of a ZnO nanocrystal and the detailed zoomed in inset image of crystallographic plains.

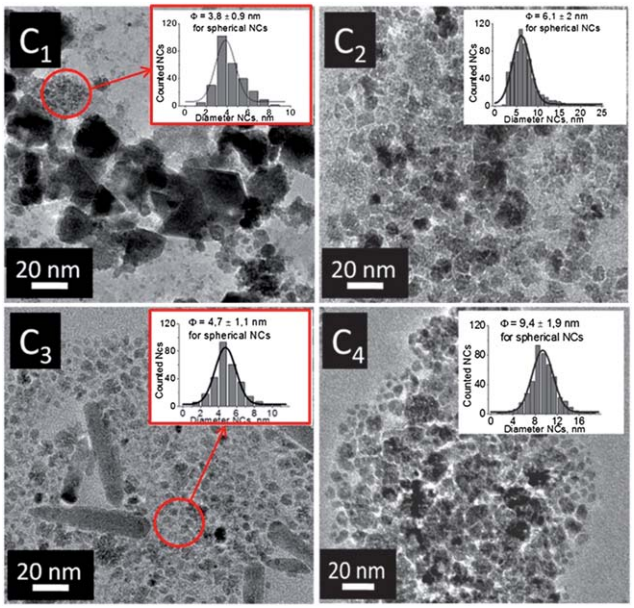

Fig. 5 HRTEM micrographs of ZnO NCs prepared with different reactor configurations (C_1–C_4). The Gaussian size distributions are shown as insets for spherical NCs.

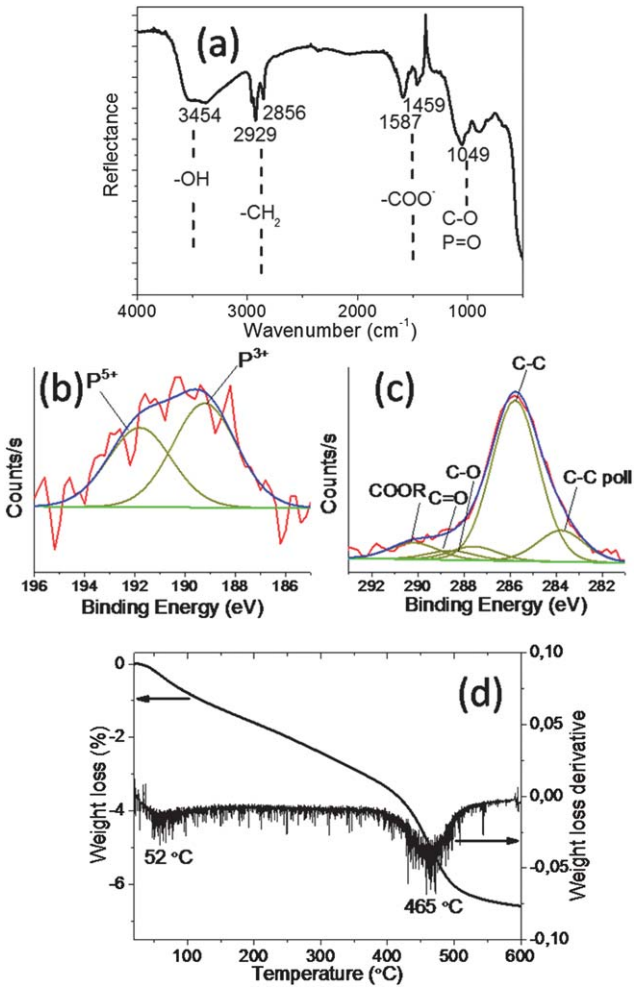

Fig. 6 FTIR (a), P_{2s} (b) and C_{1s} (c) XPS spectra and TGA (d) of ZnO NCs obtained with the C_4 millireactor.

A FTIR spectrum of ZnO NCs produced with the C_4 type reactor is shown in Fig. 6a. The strong absorption peak at 3454 cm^{-1} could be attributed to the stretching vibrations of –OH groups. The absorption peaks at 2929 cm^{-1} and 2856 cm^{-1} are stretching vibrations of the TOP's methylene groups ($-CH_2$). The peaks at 1587 and 1459 cm^{-1} are attributed to COO^- groups. The absorption peak at the position 1049 cm^{-1} could be attributed to C–O and P═O stretching vibrations. FTIR analysis shows that OH, acetylacetonate functions and also TOP molecules can be found on the surface of ZnO NCs.

XPS was performed for getting further information on the surface of ZnO NCs obtained with the C_4 millireactor. XPS analysis confirms the presence of phosphorus from TOP in two P_{2s} states (P^{3+} and P^{5+}) at 189.23 and 191.81 eV, respectively (Fig. 6b). It suggests the possible bonds between the phosphorus atoms of TOP or trioctylphosphine oxide (TOPO) with the ZnO NCs surface. The XPS spectrum also shows the presence of several contributions among which are COO^-, C═O and C–O bonds corresponding to acetylacetonate (Fig. 6c). All the above mentioned peaks disappeared upon Ar^+ ion etching of the surface, confirming the surface location of the organic functions.

TGA analysis has also been done for ZnO NCs obtained with the C_4 reactor (Fig. 6d). The TGA curve shows two weight loss steps – 0.8 and 5.9 wt%. The derivative function exhibits two peaks with global minima at 52 and 465 °C. The first peak at 52 °C can be attributed to the physisorbed traces of water from the atmosphere. The second peak at 465 °C could be attributed to the presence of chemisorbed molecules such as acetylacetonate from the precursor and TOP. The average quantity of organics around ZnO NCs is about 6 wt%.

It should be noted that the supercritical fluids based method allows obtaining of ZnO NCs with high crystallinity and as a consequence the absence of bulk and surface defects, as highlighted by the obtained PL spectra. Thereby, the supercritical fluids based method makes it possible to produce ZnO NCs with the only strong excitonic emission in the UV domain. Such unique properties of ZnO NCs of a few nm produced through the supercritical fluids route make it usable for several applications such as optochemical sensing and light emitting diodes.

Conclusions

In this paper, we obtained excitonic luminescent ZnO NCs through supercritical fluids continuous devices. We show for the first time an original methodology through the modification of reactor's size, which allows obtaining of larger quantities of ZnO NCs. Modification of the hydrodynamic profile in reactors and its control results in the production of ZnO NCs with different morphologies such as spherical NCs, triangles and nanorods. Whatever the shape of NCs, the optical properties reveal a unique excitonic UV emission which confirms that the proposed synthetic route avoids the production of visible emission traditionally observed at this scale. We believe that this type of material can be used in different types of applications such as optochemical sensing and may contribute to the improvement of the UV excitation source for light emitting diodes.

Acknowledgements

The authors acknowledge the “Région Aquitaine”, the French Research National Agency (ANR) for financial support (contract: ANR-2010-BLAN-0820) and CNRS.

Notes and references

1 Y. Hahn, *J. Chem. Eng.*, 2011, **28**, 1797.
2 L. W. Zhong, *J. Phys.: Condens. Matter*, 2004, **16**, R8029.
3 L. Schmidt-Mende and L. MacManus-Driscoll, *Mater. Today*, 2007, **10**, 40.
4 S. Anitha, B. Brabu, K. P. Rajesh and T. S. Naterajan, *Mater. Lett.*, 2013, **92**, 417.
5 C. Baratto, S. Todros, G. Faglia, E. Comini, G. Sberveglieri, S. Lettier, L. Santamaria and P. Maddalena, *Sens. Actuators, B*, 2009, **140**, 461.
6 D. M. Bagnall, Y. F. Chen, Z. Zhu, T. Yao, S. Koyama, M. Y. Shen and T. Goto, *Appl. Phys. Lett.*, 1997, **70**, 2230.
7 J. C. Johnson, Y. Haoguan, P. Yang and R. J. Saykally, *J. Phys. Chem. B*, 2003, **107**, 8816.

8 H. Hong, J. Shi, Y. Yang, Y. Zhang, J. W. Engle, R. J. Nickles, X. Wang and W. Cai, *Nano Lett.*, 2011, **11**, 3744.

9 V. Munoz-Sanjose, R. Tena-Zaera, C. Martines-Tomas, J. Zuniga-Perez, S. Hassani and R. Triboulet, *Phys. Status Solidi C*, 2005, **2**, 1106.

10 L. Vayssieres, *Adv. Mater.*, 2003, **15**, 464.

11 L. Spanhel and M. A. Anderson, *J. Am. Chem. Soc.*, 1991, **113**, 2826.

12 M. Singhal, V. Chhabra, P. Kang and D. O. Shah, *Mater. Res. Bull.*, 1997, **32**, 239.

13 Y. F. Chen, M. Kim, G. Lian, M. B. Johnson and X. G. Peng, *J. Am. Chem. Soc.*, 2005, **127**, 13331.

14 S. Kar, B. N. Pal, S. Chaudhuri and D. Chakravorty, *J. Phys. Chem. B*, 2006, **110**, 4605.

15 S. Ohara, T. Mousavand, T. Sasaki, M. Umetsu, T. Naka and T. Adschiri, *J. Mater. Sci.*, 2008, **43**, 2393.

16 A. B. Djurišić and Y. H. Leung, *Small*, 2006, **2**, 944.

17 E. Kärber, T. Raadik, T. Dedova, J. Krustok, A. Mere, V. Mikli and M. Krunks, *Nanoscale Res. Lett.*, 2011, **6**, 359.

18 C. Klingshirn, *ChemPhysChem*, 2007, **8**, 782.

19 I. M. Joni, A. Purwanto, F. Iskandar, M. Hazata and K. Okuyama, *Chem. Eng. J.*, 2009, **155**, 433.

20 S. Marre, A. Adamo, S. Basak, C. Aymonier and K. F. Jensen, *Ind. Eng. Chem. Res.*, 2010, **49**, 11310.

21 S. Marre and K. F. Jensen, *Chem. Soc. Rev.*, 2010, **39**, 1183.

22 S. Marre, Y. Roig and C. Aymonier, *J. Supercrit. Fluids*, 2012, **66**, 251.

23 Y. Roig, S. Marre, T. Cardinal and C. Aymonier, *Angew. Chem., Int. Ed.*, 2011, **50**, 12071.

24 Y. Roig, Ph.D. Thesis, University of Bordeaux 1, 2012.

25 J. Rodríques-Carvajal, *J. Phys.: Condens. Matter*, 1993, **192**, 55.

26 H. Schitz and K. H. Thiemam, *Solid State Commun.*, 1979, **32**, 783.

27 T. C. Damen, S. P. S. Porto and B. Tell, *Phys. Rev.*, 1966, **142**, 570.

28 J. H. Pan, X. Zhang, A. J. Du, H. Bai, J. Ng and D. Sun, *Phys. Chem. Chem. Phys.*, 2012, **14**, 7481.